


ARTICLE

Myosin 1b promotes axon formation by regulating actin wave propagation and growth cone dynamics

Olga Iuliano¹, Azumi Yoshimura¹, Marie-Thérèse Prospéri¹ , René Martin², Hans-Joachim Knölker² , and Evelyne Coudrier¹ 

Single-headed myosin 1 has been identified in neurons, but its function in these cells is still unclear. We demonstrate that depletion of myosin 1b (Myo1b), inhibition of its motor activity, or its binding to phosphoinositides impairs the formation of the axon, whereas overexpression of Myo1b increases the number of axon-like structures. Myo1b is associated with growth cones and actin waves, two major contributors to neuronal symmetry breaking. We show that Myo1b controls the dynamics of the growth cones and the anterograde propagation of the actin waves. By coupling the membrane to the actin cytoskeleton, Myo1b regulates the size of the actin network as well as the stability and size of filopodia in the growth cones. Our data provide the first evidence that a myosin 1 plays a major role in neuronal symmetry breaking and argue for a mechanical control of the actin cytoskeleton both in actin waves and in the growth cones by this myosin.

Introduction

Several single-headed molecular motors, myosins 1b (Myo1b), 1c, and 1d, have been identified in the brain (Sherr et al., 1993; Bähler et al., 1994; Ruppert et al., 1995; Benesh et al., 2012). Myo1b and myosin 1d are expressed in the rodent adult brain, and experimental evidence suggests that Myo1b contributes to neurogenesis (Sherr et al., 1993). Myo1b is adjacent to the plasma membrane of the growth cone in neurons from the superior cervical ganglia (Lewis and Bridgman, 1996). Transcription of *myo1b* has been correlated with the postnatal development of the mouse brain and is higher in neuroblasts from the cerebellum after their migration to the external granular layer, where they continue to divide and begin to extend two cellular processes (Sherr et al., 1993). However Myo1b function in neuronal development is not yet understood. In other cell types, Myo1b is associated with the plasma membrane and organelles (Raposo et al., 1999). Its subcellular localization is determined by a highly basic C-terminal domain (tail homology 1) containing a pleckstrin homology (PH) motif and by protein-binding partners (Salas-Cortes et al., 2005; Komaba and Coluccio, 2010; Nambiar et al., 2010; Prospéri et al., 2015; McIntosh and Ostap, 2016). Single-molecule experiments have shown that upon a resistive load, the ATP-dependent detachment of Myo1b from actin filaments (F-actin) is slowed down by two orders of magnitude (Laakso et al., 2008), suggesting that this myosin acts as a tension-sensitive motor. Given its capacity to couple the membrane to the actin cytoskeleton and generate mechanical forces, Myo1b has been proposed

to control membrane shape (Laakso et al., 2008; Nambiar et al., 2009; Almeida et al., 2011; Yamada et al., 2014). It contributes to membrane trafficking along the endocytic and exocytic pathways by controlling the shape of the organelles (Raposo et al., 1999; Nishimura et al., 2004; Salas-Cortes et al., 2005; Almeida et al., 2011; Yamada et al., 2014). Several studies also suggest that Myo1b regulates the actin architecture and participates in the formation of cell protrusions including filopodia and lamellipodia that drive cell migration (Diz-Muñoz et al., 2010; Almeida et al., 2011; Chapman et al., 2015; Ohmura et al., 2015; Prospéri et al., 2015). Given its association with neurons and its involvement in cell protrusions of other cell types, we investigate whether Myo1b contributes to cellular protrusions involved in neuronal development.

One important step in neuronal development is the establishment of polarity required for formation of the axon. Cerebellar granule neurons, cortical neurons, and hippocampal neurons first exhibit a multipolar morphology with dynamic neurites of similar size in vivo as in primary cell cultures. The fast elongation of one neurite induces neuronal polarization and specifies the axon initiation site (Bartlett and Banker, 1984a,b; Dotti et al., 1988). Studies of primary neuronal culture in vitro have shown that symmetry breaking relies on the tight spatiotemporal regulation of actin and microtubule dynamics in the growth cones, anterograde transport mediated by microtubule-associated motors and growth cone-like structures named actin waves that

¹Institut Curie, Paris Sciences et Lettres Research University, Centre National de la Recherche Scientifique, UMR 144, Paris, France; ²Department of Chemistry, Technische Universität Dresden, Dresden, Germany.

Correspondence to Evelyne Coudrier: coudrier@curie.fr.

© 2018 Iuliano et al. This article is distributed under the terms of an Attribution–Noncommercial–Share Alike–No Mirror Sites license for the first six months after the publication date (see <http://www.rupress.org/terms/>). After six months it is available under a Creative Commons License (Attribution–Noncommercial–Share Alike 4.0 International license, as described at <https://creativecommons.org/licenses/by-nc-sa/4.0/>).

propagate along the shaft of the neurites (Ruthel and Banker, 1998, 1999; Nishimura et al., 2004; Kawano et al., 2005; Jacobson et al., 2006; Toriyama et al., 2006; Flynn et al., 2009; Inagaki et al., 2011; Neukirchen and Bradke, 2011; Lewis et al., 2013; Sapir et al., 2013; Winans et al., 2016). In this study, using live-cell imaging, gene silencing, gene overexpression, and Myo1b mutants, we examine the role of Myo1b in the formation of the axon, the dynamics of the growth cone, and the actin waves. We demonstrate that the motor activity of Myo1b, and its phosphoinositides binding via its PH, are required for neuronal symmetry breaking and axon formation. We show that Myo1b controls the size of actin area in the growth cones, the propagation of actin waves, and the stability of filopodia. Collectively, our data indicate that by controlling the coupling of membrane to the actin cytoskeleton, myosin 1 regulates the organization of the F-actin network and the specification of the axon.

Results

Myo1b accumulates in growth cones

We first analyzed the expression level of Myo1b in primary culture of cortical neurons at different stages of differentiation. Neurons in culture assume different morphologies as they differentiate (Dotti et al., 1988). After dissociation and plating, embryonic cortical or hippocampal neurons are round spheres. 1 d after plating (1 d in vitro [DIV1]), they are still unpolarized and extend multiple neurites with similar length that undergo repeated stochastic elongation and retraction (stage 2). Thereafter, one of these neurites grows faster and acquires the axonal characteristics that lead to symmetry breaking (stage 3; DIV1–2). Then, the remaining short neurites form dendrites (stage 4; DIV3–4). The formation of synapses between axons and dendrites (stage 5; DIV7) and dendritic spines (stage 5–6; DIV14) completes the functional polarization of these cells. We observed that the level of Myo1b is higher between DIV1 and DIV5, the period during which the neurons undergo polarization, than later in development (compare DIV1–3 with DIV8; Fig. 1, A and B). The amount of Myo1b is reduced by >50% at DIV8 (Fig. 1, A and B). As previously reported, Myo1b appears as dots in the cell body and along the neurites up to their growth cones in stage 2 and stage 3 (DIV2) neurons with a higher concentration of Myo1b in the growth cones (Fig. 1 C; Lewis and Bridgman, 1996). We confirmed the enrichment of Myo1b in growth cones independent of the length of the neurites at DIV4 (Fig. 2 C). At this stage, axons are identified by immunolabeling with antibodies against a bona fide marker of axons, Tau-1 (Fig. 2 C). When analyzed with structural illuminated microscopy (SIM), Myo1b colocalized with F-actin in filopodia, but there was not significant overlap of Myo1b and F-actin in the interfilopodial veil of the growth cones, likely because of the association of Myo1b with the plasma membrane, whereas the F-actin network occupies a larger domain below the membrane (Fig. 1 D).

Myo1b and its motor activity are required for neuronal differentiation

Given the accumulation of Myo1b in the growth cones and its high level of expression between DIV1 and DIV5, we investigated

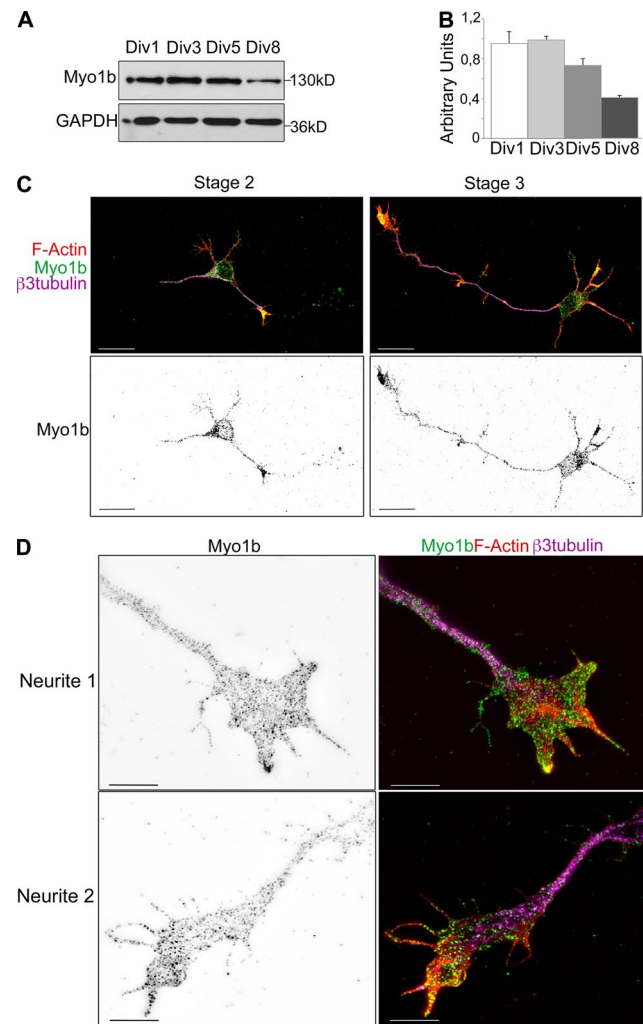


Figure 1. Distribution of Myo1b in cultured cortical neurons. (A) After 1, 3, 5, and 8 d of culture, lysates of cortical neurons were analyzed by SDS-PAGE and immunoblotting with anti-Myo1b antibodies. GAPDH was used as a loading control. (B) The amount of Myo1b detected in the lysates has been quantified as described in Materials and Methods and expressed as AU. Data are shown as the mean of three experiments. Error bars represent \pm SEM. (C) Cortical neurons DIV2 were immunolabeled with anti-Myo1b and anti- β 3-tubulin antibodies, fluorescently labeled for F-actin with phalloidin, and analyzed by confocal microscopy. A representative overlay of z stack for F-actin (red), Myo1b (green), and β 3-tubulin (magenta), and the independent z stack for Myo1b are shown for cortical neurons at stage 2 and stage 3. Bars, 20 μ m. (D) Cortical neurons DIV2 immunolabeled with anti-Myo1b and anti- β 3-tubulin antibodies and fluorescently labeled with phalloidin were analyzed by SIM. Representative images of the growth cones of one short and one long neurite labeled for Myo1b and its overlay (green) with the corresponding image for β 3-tubulin (magenta) and phalloidin (red) are shown. Bars, 5 μ m.

whether Myo1b contributes to symmetry breaking and differentiation of cortical neurons. We reduced the expression of Myo1b by 33% by transfection of Myo1b-siRNA and compared with control siRNA as judged by immunoblotting (Fig. 2, A and B). The partial reduction of Myo1b expression in neurons treated with Myo1b-siRNA, compared with the nearly complete depletion in other cell types with the same Myo1b-siRNA, likely reflects the poor efficiency of transfection in primary neuronal culture (Almeida et al., 2011; Prospéri et al., 2015). 30% of the cells transfected with

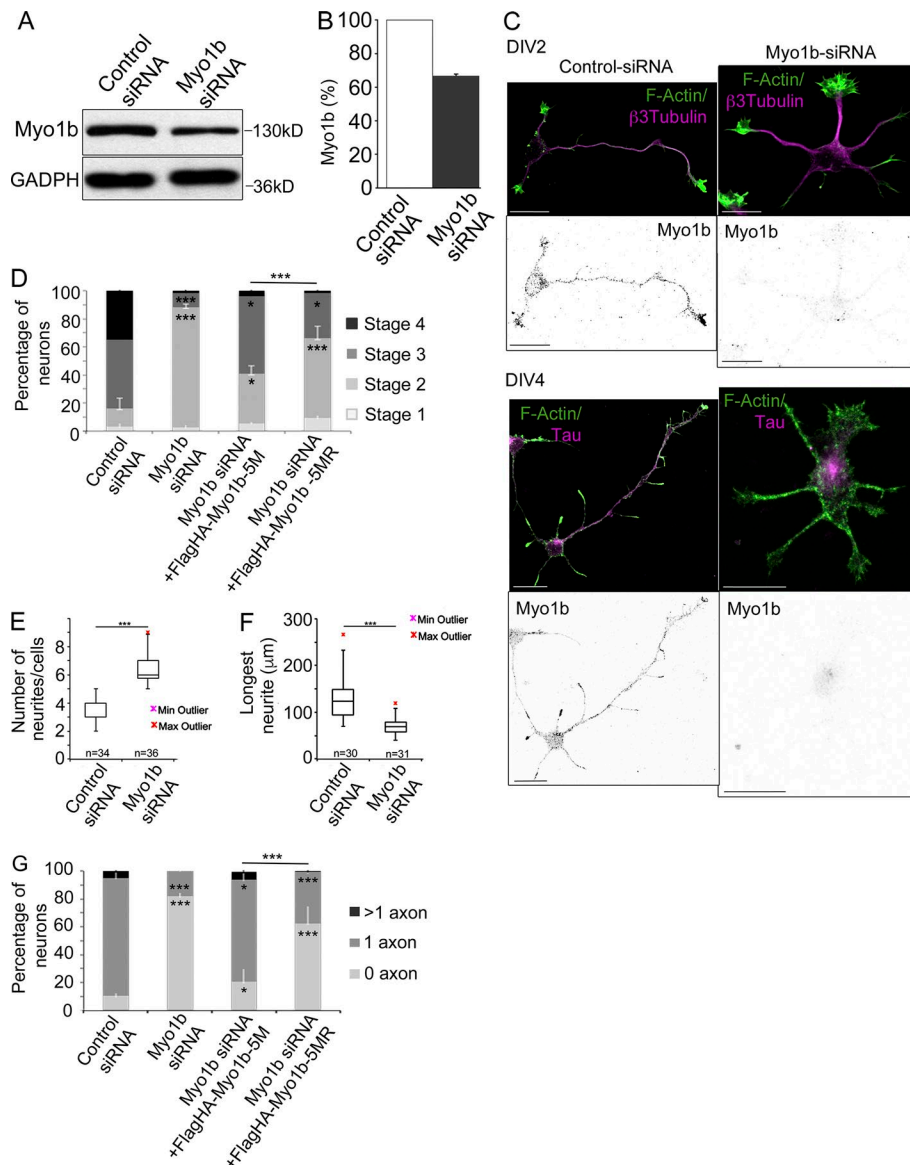


Figure 2. Depletion of Myo1b delays neuronal differentiation and inhibits the formation of axon. (A) 48 h after transfection with control or Myo1b-siRNAs, lysates of cortical neurons were analyzed by SDS-PAGE and immunoblotting with anti-Myo1b antibodies. GAPDH was used as loading control. (B) The amount of Myo1b was quantified and normalized to the amount of GAPDH. Data are shown as a mean of three experiments. (C) Cortical neurons were transfected with control or Myo1b-siRNAs, fluorescently labeled for F-actin, and immunolabeled for Myo1b and β -tubulin at DIV2 or Tau-1 at DIV4. Representative confocal z stacks for Myo1b and merged confocal z stacks for F-actin (green) and β -tubulin or Tau-1 (magenta) are shown. Bars, 20 μ m. (D) The percentages of neurons showing each of the different stages of differentiation were quantified for neurons transfected with control siRNAs, Myo1b-siRNA, Myo1b-siRNA+Flag-HA-Myo1b5M, and Myo1b-siRNA+Flag-HA-Myo1b5MR based on their morphologies observed at DIV2 after immunolabeling for β -tubulin and fluorescently labeled for F-actin. Data are shown as the mean of three independent experiments for each condition. Error bars represent \pm SEM. $n = 30$ cells/experiment. (E) The number of neurites per cell was quantified in cortical neurons transfected with control siRNA or Myo1b-siRNA at DIV2 and represented as box plots. $n = 3$ independent experiments; $n = 30$ cells/experiment. (F) The length of the longest neurite in cortical neurons transfected with control siRNA or Myo1b-siRNA was measured at DIV2 and represented as box plots. $n = 3$ independent experiments; $n = 30$ cells/experiment. (G) The percentages of neurons with none, single, and multiple axons were quantified after transfection of control and Myo1b-siRNAs, Myo1b-siRNA+FlagHA-Myo1b-5M, or Myo1b-siRNA+FlagHA-Myo1b-5MR and immunolabeling at DIV4 for Tau-1 to identify nascent axons. Data are shown as the mean of three independent experiments for each condition. Error bars represent \pm SEM. $n = 30$ cells/experiment. Data distribution was assumed to be normal. χ^2 test (D and G); unpaired t test (F and G). *, $P < 0.05$; **, $P < 0.01$; ***, $P < 0.0001$.

Myo1b siRNA did not show specific Myo1b immunolabeling. In the following analyses, we only examined the neurons that were negative for Myo1b. The majority of Myo1b-negative neurons at DIV2 and DIV4 were unpolarized. Neurites had similar size, but Tau-1 was detected only in the cell bodies of Myo1b-negative neurons at DIV4 (Fig. 2 C). We compared the percentage of neurons exhibiting different stages of differentiation after transfection of Myo1b-siRNA or control siRNA at DIV2. Myo1b depletion increased by >60% the percentage of nonpolarized stage 2 neurons compared with neurons transfected with control siRNA (Fig. 2 D). Furthermore, it increased the number of neurites per cell by almost twofold (Fig. 2 E) and decreased the length of the longest neurite by 50% (Fig. 2 F). To confirm the impact of Myo1b depletion on the formation of the axon, we quantified at DIV4 the proportion of neurons showing none, single, or multiple

axons in cortical primary cultures transfected with control or Myo1b-siRNAs and as judged by the distribution of Tau-1. Myo1b depletion decreased by 70% the percentage of cells with single Tau-1-labeled protrusions (Fig. 2 G). These defects were rescued by expressing FlagHA-Myo1b-5M, which is resistant to Myo1b-siRNA (Fig. 2, D and G), confirming the specificity of our knock-down (Almeida et al., 2011). We next determined whether Myo1b motor activity was required for the formation of the axon. We have previously designed and characterized in vivo and in vitro a Myo1b rigor mutant, FlagHA-Myo1b-5MR, by introducing the mutation N160A in the ATPase pocket of FlagHA-Myo1b-5M (Almeida et al., 2011). Expression of this construct was much less effective in rescuing the formation of polarization of the neurons and differentiation of the axon (Fig. 2, D and G). Collectively, these observations indicate that the motor activity of Myo1b is

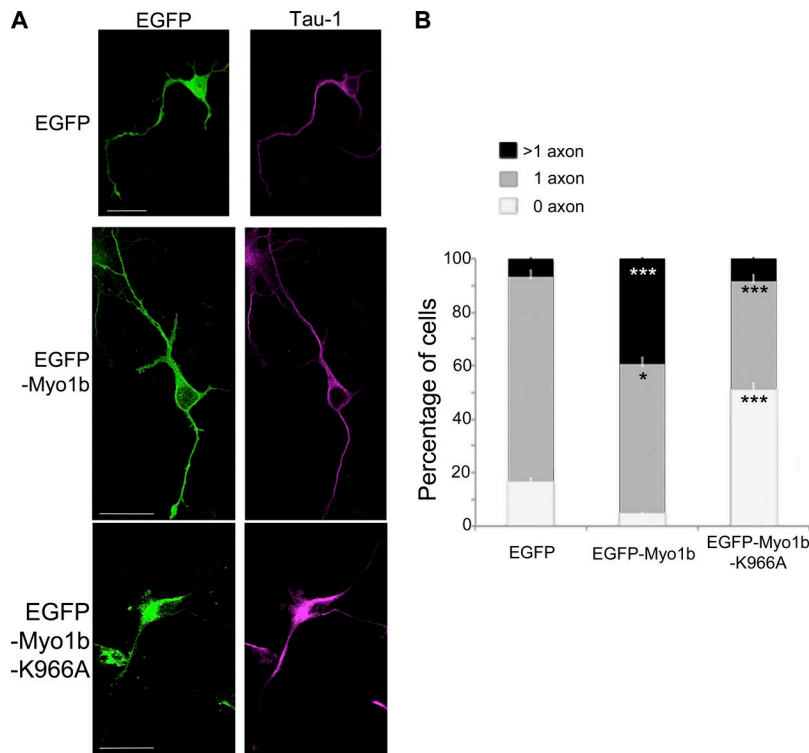


Figure 3. Myo1b overexpression induces multiple axon-like processes and requires the integrity of its PH motif. (A) Cortical neurons transfected with plasmids encoding EGFP, EGFP-Myo1b, and EGFP-Myo1b-K966A were immunolabeled for Tau-1 to identify nascent axons at DIV4 and analyzed by confocal microscopy. Representative z stacks are shown. Bars, 20 μ m. (B) The percentages of neurons with none, single, or multiple axons were quantified after transfection of plasmids encoding EGFP, EGFP-Myo1b, and EGFP-Myo1b-K966A and immunolabeling at DIV4 for Tau-1. Data are shown as the mean of three independent experiments for each condition. Error bars represent \pm SEM. $n = 30$ cells/experiment. Data distribution was assumed to be normal. χ^2 test. *, $P < 0.05$; ***, $P < 0.001$.

required for the establishment of neuronal polarity and the formation of the axon.

The PH motif of Myo1b is required for neuronal differentiation

The Myo1b PH motif contributes to its binding to the plasma membrane (Komaba and Coluccio, 2010). We thus wondered whether this motif was necessary for the formation of the axon. We compared the percentage of neurons with none, one, or multiple axons in neurons that expressed EGFP, EGFP-Myo1b, or EGFP-Myo1b-K966A, a mutant with a single mutation in the PH motif that inhibits its binding to phosphoinositides (Komaba and Coluccio, 2010). Consistent with the role of Myo1b in the formation of the axon, the expression of EGFP-Myo1b increases by more than fivefold the percentage of neurons with multiple axon-like protrusions positive for Tau-1 compared with the expression of EGFP (Fig. 3, A and B). In contrast with EGFP-Myo1b, the expression of EGFP-Myo1b-K966A does not increase the percentage of neurons with multipolar Tau-1-positive protrusions (Fig. 3, A and B). It even decreases the percentage of cells with one axon compared with the expression of EGFP, suggesting that the binding of Myo1b to the plasma membrane via its interaction with phosphoinositides is necessary for the symmetry breaking and the formation of the axon (Fig. 3 B).

Growth cones and actin waves share similar actin structures

Symmetry breaking and axon formation rely on the fast outgrowth of one neurite. This fast outgrowth has been correlated with important changes in the morphology of the growth cone, including the dynamic assembly and disassembly of F-actin in the peripheral domain (P-domain) of the growth cones (Bradke and Dotti, 1999; Ren and Suter, 2016). Actin waves are also important contributors to the formation of the axon. They are

actin structures that propagate along the shaft of the neurites in contacting and deforming the plasma membrane (Flynn et al., 2009). The fusion of the actin waves with the tip of the neurite correlates with neurite growth (Ruthel and Banker, 1998, 1999; Flynn et al., 2009). Because they occur more frequently in the future axon during the initial neuronal polarization and their arrival at the growth cone coincides with a burst of axon elongation, they have been suggested to promote axogenesis (Flynn et al., 2009). Several studies suggest that actin waves have a similar molecular composition and similar dynamics as growth cones (Ruthel and Banker, 1998, 1999; Flynn et al., 2009). We confirmed the important similarity between the growth cones and the actin waves by comparing their actin structure with SIM and high-resolution EM using platinum replica (Fig. 4). As previously reported for the growth cones, F-actin bundles form filopodia and a dense F-actin meshwork that connects the rootlets of the F-actin bundles in the interfilopodial veil in the actin waves (Korobova and Svitkina, 2008). We thus questioned whether the manipulation of the expression of Myo1b impacts the dynamics of growth cones and the actin waves.

Myo1b promotes anterograde propagation of the actin waves

We first investigated whether Myo1b is associated with actin waves. Endogenous Myo1b colocalizes with actin structures that induce membrane deformation along the neurites of neurons as observed by SIM (Fig. 5 A). Furthermore, the propagation of LifeAct-EGFP along the neurite shaft correlates with the propagation of mCherry-Myo1b (Fig. 5 B and Video 1). During their propagation along the neurite shaft, actin waves interact with the plasma membrane and induce locally its deformation. Phosphatidylinositol-3,4,5-triphosphate (PIP3), one of the phosphatidylinositols associated with the plasma membrane, localizes

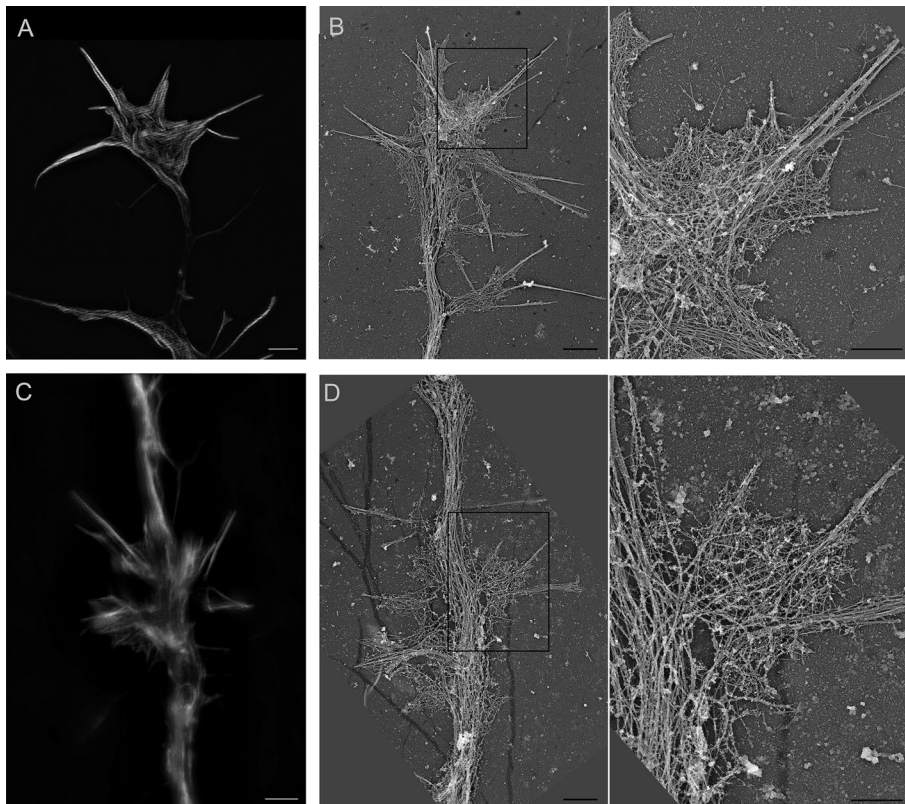


Figure 4. Growth cones and actin waves share important structural similarities. (A–D) Distribution of F-actin cytoskeleton of growth cones (A and B) and actin waves (C and D) of DIV2 cortical neurons visualized by SIM (A and C) and platinum replica EM (B and D). Boxed regions in B and D are enlarged in the right panel. Bars: (A–D, left) 2 μ m; (B and D, right) 1 μ m.

with actin waves (Kakumoto and Nakata, 2013). Interestingly, the propagation of mCherry-Myo1b is correlated with that of the endogenous PIP3 when detected by the expression of Akt-PH-EGFP (Fig. 5 C and Video 2). Collectively, these observations indicate that Myo1b is associated with actin waves.

We then examined whether Myo1b expression controls the formation and/or the propagation of the actin waves at DIV1 in stage 2 unpolarized neurons. The number of actin waves per neurite within 1 h varied depending on cell cultures (Fig. 6, C, E, and G). However, Myo1b depletion or overexpression did not change this number when compared with control performed using the same cell culture (Fig. 6, C and G). In contrast, the depletion of Myo1b by siRNA inhibited the anterograde propagation of these actin waves when compared with the neurons transfected with control siRNA in the same set of experiments (Fig. 6, A, B, and D; and Video 3). In control siRNA-transfected neurons, 82.9% of the actin waves propagated toward the tip of the neurites (anterograde waves) and 4.8% toward the cell body (retrograde waves), and 12.3% were abortive. In Myo1b-siRNA-transfected neurons, however, only 11.1% of the waves were anterograde, and 77.4% were abortive (Fig. 6 D). Furthermore, experiment showed that Myo1b motor activity and its ability to bind membrane via its PH motif were both required for the propagation of the anterograde actin waves. The number of actin waves per neurite was similar after treatment with the myosin 1 inhibitor pentachloropseudilin (PCLP) compared with the diluent (Fig. 6 E) or after expression of mCherry-Myo1b-K966A compared with mCherry (Fig. 6 G; Chinthalapudi et al., 2011). However, 59.4% of the actin waves were abortive in cells treated with PCLP compared with 10.3% in the presence of

the diluent (Fig. 6 F). The expression of mCherry-Myo1b did not affect significantly the percentage of anterograde waves compared with the expression of mCherry (Fig. 6 H), whereas only 13% of the waves were anterograde in neurons expressing mCherry-Myo1b-K966A compared with 80% and 68% in neurons expressing mCherry or mCherry-Myo1b, respectively (Fig. 6 H). Collectively, these observations indicate that Myo1b is required to direct the anterograde propagation of actin waves to the tip of the neurites but not for their initial formation. Myo1b motor activity and the integrity of its PH motif are both necessary for this function.

Myo1b impacts dynamics of Kif5C⁵⁶⁰, an early axonal marker

The kinesin 1 Kif5C dynamically shuttles from one neurite to another in unpolarized neuron stage 2 before accumulating at the tip of one neurite coincident with axon specification. The minimal motor domain of Kif5C⁵⁶⁰-EGFP that is constitutively active has thus been considered as an early axonal marker in several studies (Jacobson et al., 2006; Randlett et al., 2011). Recently, Winans et al. (2016) have shown that actin waves are linked to microtubule polymerization and thereby control the stochastic fluctuation of Kif5C. These observations collectively suggest that by regulating actin waves, Myo1b may impact indirectly the stochastic fluctuation of Kif5C and thereby axon specification. To test this hypothesis, we analyzed the behavior of Kif5C⁵⁶⁰-EGFP depending on the expression of Myo1b using mCherry tag shRNAs. Similar to siRNA, the expression of Myo1b was reduced by only 35% after transfection of the plasmid encoding Myo1b mCherry-shRNA when analyzed by Western blot (Fig. S1, A and B), corresponding with a mean of 30% of the cells expressing the

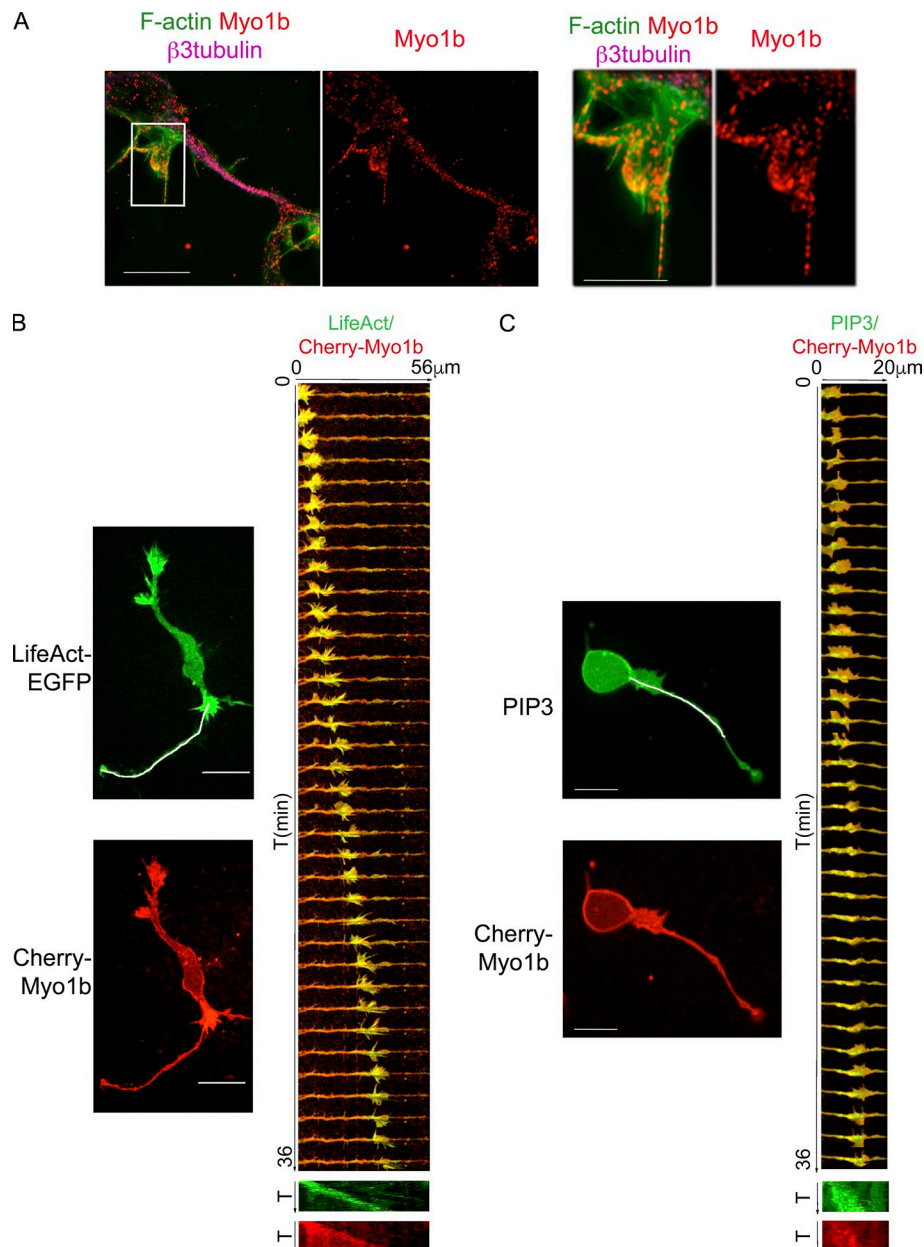


Figure 5. Myo1b is associated with and propagates with actin waves. (A) Merged fluorescence images acquired with SIM of an actin wave costained with anti-Myo1b antibodies, Alexa Fluor 488 phalloidin, and anti- β 3-tubulin antibody and images of the 2.5 \times enlargement of the region marked by a white box are shown. (B) The propagation of F-actin structures and mCherry-Myo1b has been analyzed in cortical neurons expressing LifeAct-EGFP and mCherry-Myo1b at DIV1 by time-lapse spinning confocal microscopy. The first frame of Video 1 (one frame per minute) for LifeAct-EGFP and mCherry-Myo1b and the merged kymographs of 36 frames for the region marked on the first frame by a white lane for the two recombinant proteins are shown. The increase of fluorescence intensity for LifeAct-EGFP correlated with the increase of fluorescence intensity for mCherry-Myo1b. (C) The propagation of PIP3 and mCherry-Myo1b has been analyzed in cortical neurons expressing AKT-PH-EGFP and mCherry-Myo1b at DIV1 by time-lapse spinning confocal microscopy. The first frame of Video 2 and kymographs of 36 frames for the region marked on the first frame by a white lane for the two recombinant proteins are shown. The increase of fluorescence intensity for AKT-PH-EGFP correlated with the increase of fluorescence intensity for mCherry-Myo1b. Bars: (A) 10 μ m; (B and C) 20 μ m. T, time

mCherry tag. Nevertheless, the advantage of the transfection with plasmids encoding mCherry-shRNAs is that the transfected neurons can be identified *in vivo* because of the mCherry tag. We observed that Kif5C⁵⁶⁰-EGFP switched from one neurite to another, moving back and forth along the neurite shaft and accumulating transiently at the tip of one neurite in nonpolarized stage 2 neurons expressing control mCherry-shRNA (Fig. 7 A and Video 4 a). In contrast, Kif5C⁵⁶⁰-EGFP remained primarily in the cell body of neurons expressing Myo1b-mCherry-shRNA and did not show any stochastic movement from one neurite to another (Fig. 7 A and Video 4 b). In contrast, we observed accumulation of Kif5C⁵⁶⁰-EGFP at the tips of the different neurites in neurons expressing mCherry-Myo1b (Fig. 7 B and Video 5). Thus, by regulating the anterograde migration of the actin waves, Myo1b influences the stochastic fluctuation of Kif5C from one neurite to another.

Myo1b regulates the spreading of the growth cones and the size of the P-domain containing F-actin

We next analyzed the impact of Myo1b expression on the behavior of the growth cone. We first compared by phase contrast live-cell imaging the dynamic changes of the growth cone morphology in neurons transfected with control or Myo1b-siRNA. In these experiments, we analyzed only unpolarized stage 2 cells at DIV1. The growth cones of the neurons transfected with control siRNA spread and contracted, whereas the neurites elongated (Video 6 a). In contrast, the growth cones of Myo1b-depleted neurons remained widely spread, and the neurites rarely elongated (Video 6 b). The area of the growth cones of all the neurites of neurons transfected with Myo1b-siRNA significantly increased within 1 h. In contrast, it decreased in neurons transfected with control siRNA, likely because of the increased area of only the growth cone of the future axon (Fig. S2, A and B; and Video 6, a

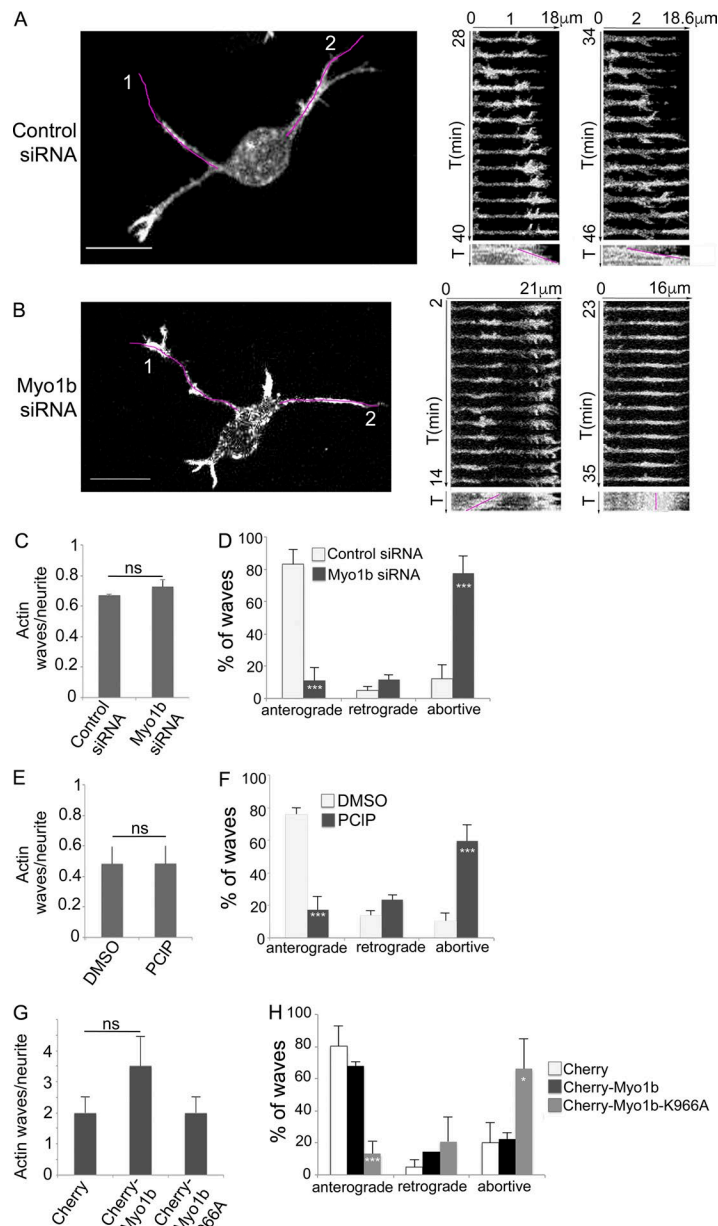


Figure 6. Myo1b, its motor activity, and its PH motif control the anterograde propagation of actin waves. (A and B) The propagation of actin waves has been analyzed in cortical neurons transfected with control (A) or Myo1b-siRNAs (B) at DIV1 by time-lapse spinning confocal microscopy (see also Video 3, a and b). Images of the first frame and the kymographs of the Video 6 (a and b) for the region marked by a purple lane on the first frames for 13 min are shown (time lapse, 1 min). T, time. Two anterograde waves are observed in control cells (A1 and A2), whereas in Myo1b-depleted neurons, actin waves are formed, but they either migrate to the cell body (retrograde; B1) or oscillate and collapse along the shaft of neurite (B2). Bars, 10 μ m. **(C and D)** Ratio of actin waves per neurite (C) and anterograde, retrograde, and abortive actin waves normalized to the total number of waves (D) observed by time-lapse spinning confocal microscopy in cells cotransfected with LifeAct-EGFP and control or Myo1b-siRNA. Data are shown as the mean of three independent experiments for each condition. $n = 13, 9$, and 6 cells for control siRNA treatment; $n = 9, 8$, and 3 cells for Myo1b-siRNA treatment per experiments. **(E and F)** Ratio of actin waves per neurite (E) and anterograde, retrograde, and abortive waves normalized to the total number of waves (F) observed by time-lapse spinning confocal microscopy in cells transfected with LifeAct-EGFP and treated with DMSO or PCIP. Data are shown as the mean of three independent experiments for each condition. $n = 11, 17$, and 7 for PCIP treatment per experiment. **(G and H)** Ratio of actin waves/neurite (G) and anterograde, retrograde, and abortive actin waves normalized to the total number of waves (H) observed in neurons transfected with LifeAct-EGFP together with mCherry, mCherry-Myo1b, or mCherry-Myo1b-K966A. Data are shown as the mean of three independent experiments for each condition. $n = 6, 10$, and 7 cells expressing mCherry; $n = 7, 11$, and 10 cells expressing mCherry-Myo1b; $n = 11, 8$, and 8 cells expressing mCherry-Myo1b-K966A per experiment. Data distribution was assumed to be normal. χ^2 test. *, $P < 0.05$; ***, $P < 0.001$.

and b). We then studied whether the enlargement of the growth cones in Myo1b-depleted cells corresponds with an increase of F-actin in the P-domain. Indeed, in Myo1b-depleted cells, the area positive for F-actin increased by 50% in the growth cones, compared with neurons transfected with control siRNA (Fig. 8, A and B). We also probed whether the ability of Myo1b to bind the plasma membrane via its PH motif impacted F-actin in the P-domain. We compared the impact of EGFP-Myo1b and EGFP-Myo1b-K966A expressions with EGFP expression for the size of the P-domain. The area of the growth cone positive for F-actin was reduced by 70% in neurons expressing EGFP-Myo1b compared with neurons expressing EGFP (Fig. 8, C and D), and microtubules were often observed to the tip of the neurites (Fig. 8 C; inset). In contrast, expression of EGFP-Myo1b-K966A reduced by only 50% the F-actin area (Fig. 8, C and D). The significant intermediate size of the P-domain in neurons expressing EGFP-Myo1b-K966A compared with neurons expressing EGFP or EGFP-Myo1b suggests

that the binding of Myo1b to the plasma membrane contributes to the size of the F-actin area in the growth cones. Collectively these observations indicate that Myo1b and its ability to bind the plasma membrane regulate the morphology of the growth cones and the size of the P-domain containing F-actin.

Myo1b contributes to filopodia stability and their F-actin density

We then examined actin dynamics in growth cones of multipolar neurons at DIV1 after the expression of mGFP-F-tractin-P and depletion of Myo1b using si- or shRNAs. The interfilopodial veil and filopodia extended and retracted, and occasionally filopodia coalesced in growth cones of neurons transfected with control siRNA or shRNA (Videos 7 a and 8 a). In contrast, in neurons transfected with Myo1b-siRNAs or -shRNAs, the interfilopodial veil appeared to extend more than in control cells (Fig. 9, A, B, F, and G; and Videos 7 a and 8 a). The number of filopodia observed

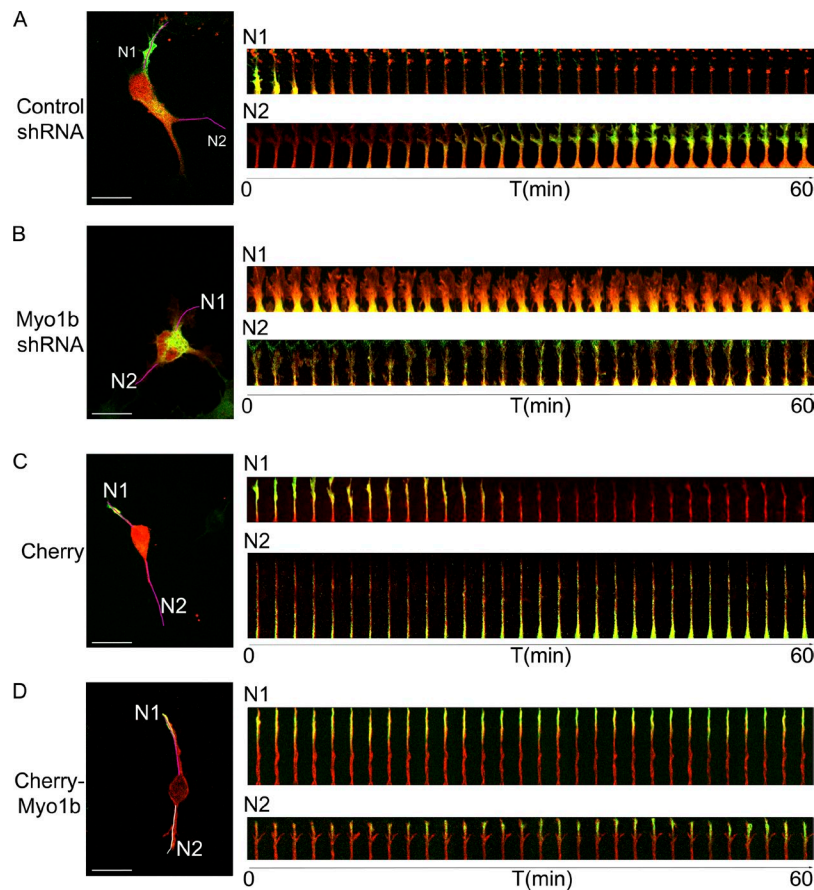


Figure 7. Myo1b expression regulates the trafficking of Kif5C⁵⁶⁰ in neurites. The dynamics of Kif5C⁵⁶⁰ have been analyzed by time-lapse spinning confocal microscopy in cells expressing Kif5C⁵⁶⁰-EGFP and control or Myo1b-mCherry-shRNA at DIV1 (A and B) or mCherry or mCherry-Myo1b (C and D). The merged first frames and the merged kymograph (one frame/2 min) for Kif5C⁵⁶⁰-EGFP (green) and mCherry (red) of the Video 4 (a and b) for shRNAs and Video 5 (a and b) for mCherry and mCherry-Myo1b are shown. T, time. Bars, 20 μ m. The purple lines on the first frame mark the regions for which the kymographs illustrate the dynamics of Kif5C⁵⁶⁰ within 1 h.

within 3 min was not affected by Myo1b depletion (Fig. 9, C and H), but filopodia were significantly shorter (Fig. 9, A, B, D, and I). Their length decreased by 25% regardless of the method to reduce Myo1b expression (Fig. 9, D and I), and they elongated less frequently in cells expressing Myo1b shRNA than in control cells (Fig. 9 K). In addition, the lifespan of the filopodia decreased because of an increase of coalescence frequency (Videos 7 and 8; and Fig. 9, E and J). Filopodia in actin waves were also less stable in cells transfected with Myo1b-siRNA or -shRNA (Fig. S3 and Videos 9 and 10). Collectively these observations indicate that Myo1b contributes to the stability of the filopodia in both growth cones and actin waves.

We next analyzed more deeply the impact of Myo1b expression on the architecture of F-actin in the growth cone. We measured the fluorescent intensity of F-actin in filopodia and analyzed actin organization in growth cones depending on Myo1b expression by confocal microscopy or SIM. Myo1b depletion by shRNA significantly decreased F-actin in filopodia compared with the interfilopodial veils when visualized after expression of mGFP-F-tractin-P (Fig. 10, A and C). Analysis of the actin network by SIM revealed more abundant actin bundles inside the interfilopodial veil and short filopodia in growth cones of Myo1b-depleted neurons compared with the growth cones of cells expressing control mCherry-shRNA (Fig. 10 C). Moreover, fluorescence intensity in the filopodia compared with that in the total growth cones was significantly decreased by 33% (Fig. 10 B). This decrease compared with the 25% reduction of the length of the filopodia in the same experimental conditions (Fig. 9 I)

suggests that Myo1b controls the thickness of F-actin bundles in filopodia as well as their length. Collectively, these observations indicate that Myo1b regulates the organization of F-actin in the growth cone by controlling the size of the F-actin-containing P-domain, including filopodia and the interfilopodial veils, and the stability of the filopodia.

Discussion

The previous analysis of the distribution of Myo1b and its mRNA in brain and in neurons suggested a possible function of Myo1b for neuronal development (Sherr et al., 1993; Lewis and Bridgman, 1996). We show that Myo1b triggers the establishment of neuronal polarity as documented by the differentiation of a single neurite into an axon. The formation of the axon relies on the fast outgrowth of one among several neurites that depends on actin instability in the growth cone and the propagation of the actin waves. We observed that actin waves and growth cones share F-actin arrays with similar architectures. Furthermore, in agreement with previous observations showing that growth cones and actin waves contain the same actin-binding proteins (Ruthel and Banker, 1998, 1999; Flynn et al., 2009), our work indicates that Myo1b is another common constituent of both structures.

A myosin 1 has been previously reported to be associated with actin waves in *Dictyostelium discoideum* (Brzeska et al., 2014). We now report the first evidence that a myosin 1 contributes to the direction of the propagation of the actin waves in mouse primary neurons. Myo1b propagates along the neurites with F-actin and

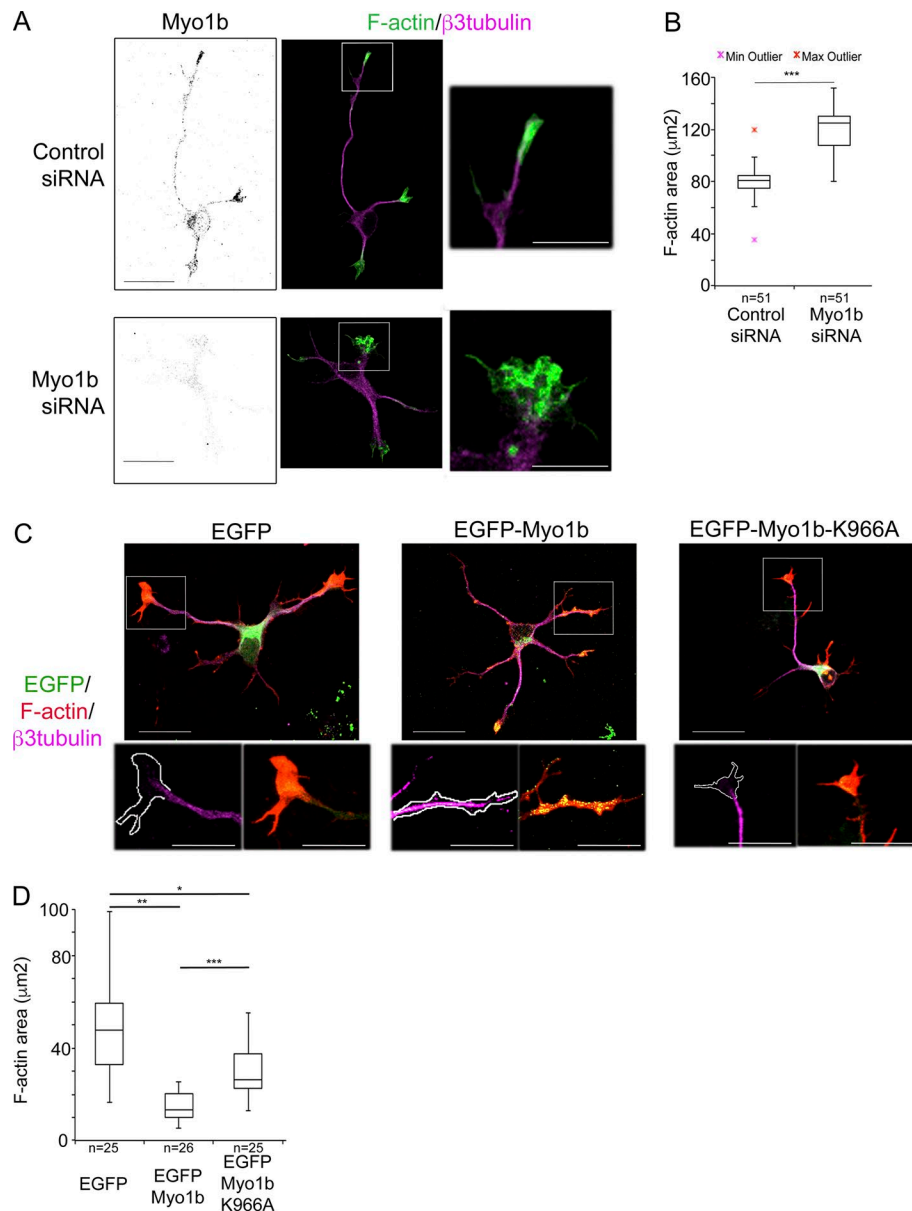


Figure 8. Myo1b controls the size of the F-actin-enriched area in the growth cones.

(A) Cortical neurons were transfected with control or Myo1b-siRNAs, immunolabeled for Myo1b and β 3-tubulin, and fluorescently labeled for F-actin at DIV2. Representative confocal z stacks for Myo1b, merged confocal z stacks for F-actin (green) and β 3-tubulin (magenta), and images of the 3 \times enlargements of the regions marked by the white boxes are shown. **(B)** The measurements of the area occupied by F-actin in the growth cone of the longest neurite as judged by β 3-tubulin labeling in cells transfected with Myo1b- or control siRNAs are represented as box plots. $n = 51$ in three independent experiments. **(C)** Cortical neurons expressing EGFP, EGFP-Myo1b, or EGFP-Myo1b-K966A, immunolabeled for β 3-tubulin, and fluorescently labeled for F-actin at DIV2. Representative merged confocal z stacks for EGFP (green), β 3-tubulin (magenta), and F-actin (red) and images of the 2.5 \times enlargements of the regions marked by the white boxes are shown. Bars, 20 μm . **(D)** The measurements of the area occupied by F-actin in the growth cone of the longest neurite as judged by β 3-tubulin labeling in cells expressing EGFP, EGFP-Myo1b, or EGFP-Myo1b-K966A are represented as box plots. $n = 25$ in three independent experiments. Data distribution was assumed to be normal. Unpaired t test. *, $P < 0.05$; **, $P < 0.01$; ***, $P < 0.001$.

PIP3, two major components of the actin waves. As reported for the myosin 1 of *Dictyostelium*, we have detected accumulation of the endogenous Myo1b at the front of some waves in fixed cells (Brzeska et al., 2014). Furthermore, Myo1b depletion inhibits the anterograde propagation of the actin waves that has been shown to contribute to neurite elongation. It has been recently shown that, by enlarging the shaft of the neurites, actin waves control microtubule polymerization and the microtubule-based transport of proteins involved in axon specification such as shootin and slingshot (Winans et al., 2016). In agreement with these observations, we have shown that depletion of Myo1b, in addition to perturbing the anterograde propagation of the actin waves, also perturbs the stochastic movements of Kif5C, a microtubule-associated motor that transports proteins involved in axon specification. Thus, Myo1b may trigger the axon specification indirectly by regulating the anterograde propagation of the actin waves and thereby the KIF5C-dependent delivery of axon-promoting factors to the tip of the future axon.

It is unlikely that the contribution of Myo1b to anterograde migration of the actin waves consequently impacts the actin network in the growth cones. Indeed, the F-actin-containing P-domain of the growth cone was enlarged in Myo1b-depleted cells, whereas anterograde propagation of the actin waves was inhibited, which is expected to reduce F-actin in this region. In contrast, overexpression of Myo1b increased the percentage of cells with axon-like protrusions and decreased the size of the F-actin network in the growth cones. Nevertheless, it did not disturb the actin wave propagation, whereas it induced the accumulation of Kif5C at the tip of the neurites. This suggests that overexpression of Myo1b perturbs the distribution of the microtubules via another means. According to a previous study, disruption of the actin network in the growth cone produced neurons with multiple axon-like protrusions because of microtubule polymerization extending to the tip of the neurites (Bradke and Dotti, 1999). Indeed, we observed that the important reduction of the actin network in the growth cones resulting from overexpression of

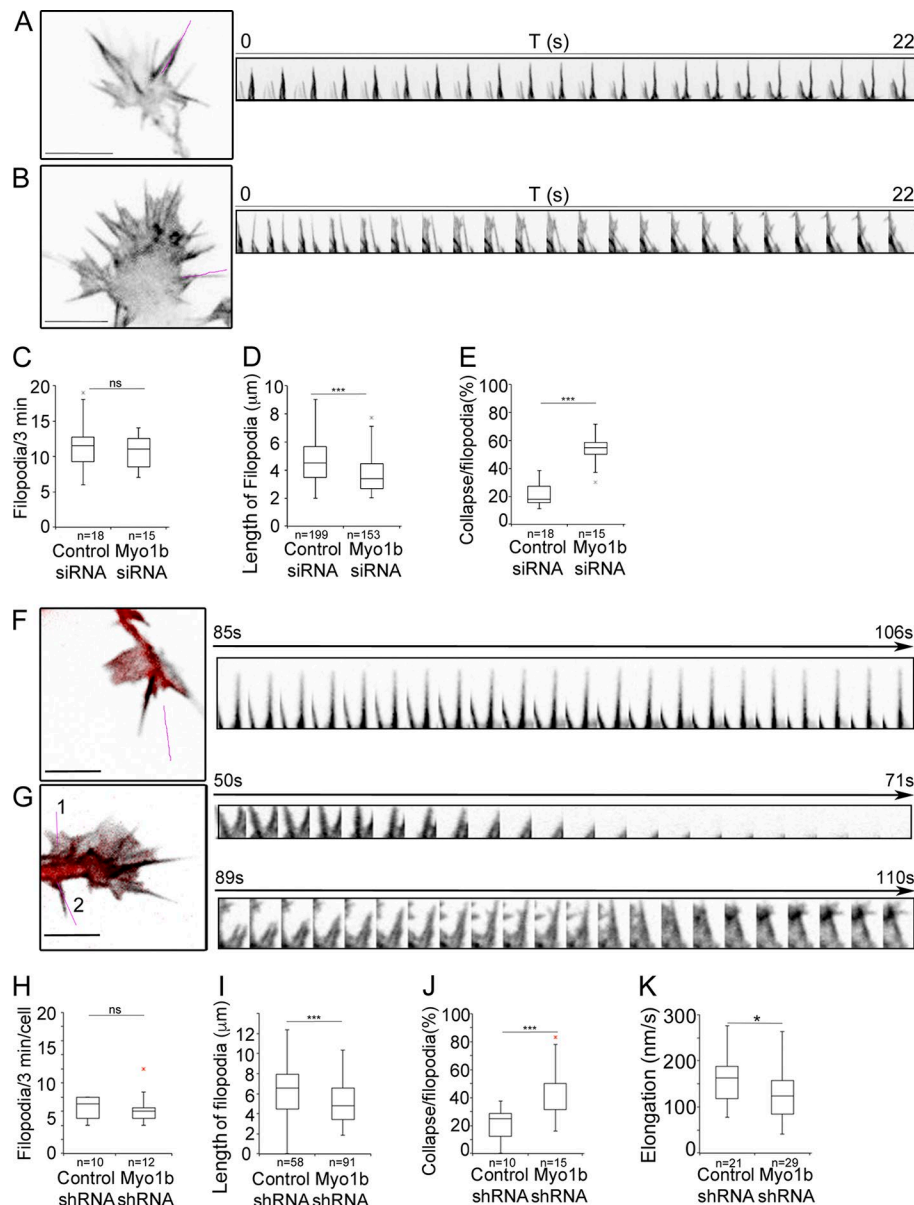


Figure 9. Depletion of Myo1b affects the length and lifespan of filopodia. (A–E) Cortical neurons transfected with plasmid encoding mGFP-F-tractin-P and control siRNA (A) or Myo1b-siRNA (B) were analyzed at DIV1 during 3 min (one frame/s) using spinning confocal microscopy. Images of the first frames of Video 7 (a and b) and the kymographs of 22 frames for the region marked by a purple lane are shown. Note that the two filopodia in a Myo1b-depleted cell collapse within 22 s, whereas those in the control cell remain stable. The ratio of filopodia per growth cone observed within 3 min ($n = 18$ or 15 ; C), the length of the filopodia ($n = 199$ or 153 ; D), and the ratio of filopodia per growth cone collapsing within 3 min ($n = 18$ or 15 ; E) have been quantified and represented as box plots for three independent experiments. T, time. (F–K) Cortical neurons expressing mGFP-F-tractin-P and control mCherry-shRNA (F) or Myo1b-mCherry-shRNA (G) were analyzed at DIV1 for 3 min (one frame/s) using spinning confocal microscopy. Merged images of the first frames of Video 8 (a and b) showing F-actin (gray) and mCherry (red) in the growth cone are shown. The magenta lanes mark the regions for which kymographs of the dynamics of filopodia for 22 s are shown. Bars, $13\ \mu\text{m}$. The ratio of filopodia per growth cone observed within 3 min ($n = 10$ or 12 ; H), the length of the filopodia ($n = 58$ or 91 ; I), the ratio of filopodia per growth cone collapsing within 3 min ($n = 10$ or 15 ; J), and the velocity of the elongation ($n = 21$ or 29 ; K) have been quantified and represented as box plots in three independent experiments. Data distribution was assumed to be normal. Unpaired t test. **, $P < 0.01$; ***, $P < 0.001$.

Myo1b favors the presence of microtubules to the tips of neurites. Thus, overexpression of Myo1b may lead to the formation of multiple axon-like structures by increasing the instability of F-actin in the growth cone and consequently facilitating microtubule polymerization and Kif5C accumulation at the tip of the neurites. In contrast, reduced expression of Myo1b that we showed to increase the size of the actin network in the growth cone may increase F-actin stability in the growth cones. These observations collectively underline the impact of Myo1b on the organization of F-actin in the growth cone, which is of key import for axon formation.

Expression of Myo1b PH mutant did not induce the formation of multiple axon-like structures and did not reduce the size of the F-actin network in the growth cone as much as Myo1b overexpression, suggesting that the instability of F-actin in the growth cones induced by Myo1b overexpression required its interaction with the plasma membrane. However, expression of this mutant increased the percentage of cells that do not form axons and

perturbed the anterograde migration of actin waves. Because of its inability to interact with PIP2, the PH mutant was principally in the cytoplasm. It may consequently perturb to some extent the organization of F-actin in the growth cone and the actin waves and therefore their propagation. Collectively, our observations strongly suggest that by coupling F-actin to the membrane Myo1b regulates actin architecture both in the growth cone and in actin waves.

Depletion of Myo1b decreased the lifespan of filopodia present in both actin waves and growth cones, reduced their length, and reduced the density of F-actin in filopodia of the growth cones. It is largely accepted that by sensing attractive or repulsive cues and exploring adhesive surface, filopodia determine the direction of growth cone movement. Similarly, they may control the orientation of actin wave migration. Transformation of actin polymerization into a protrusion requires interaction of F-actin with the plasma membrane. Given their ability to bind membrane phosphoinositides, myosins 1 are good candidates to fulfill

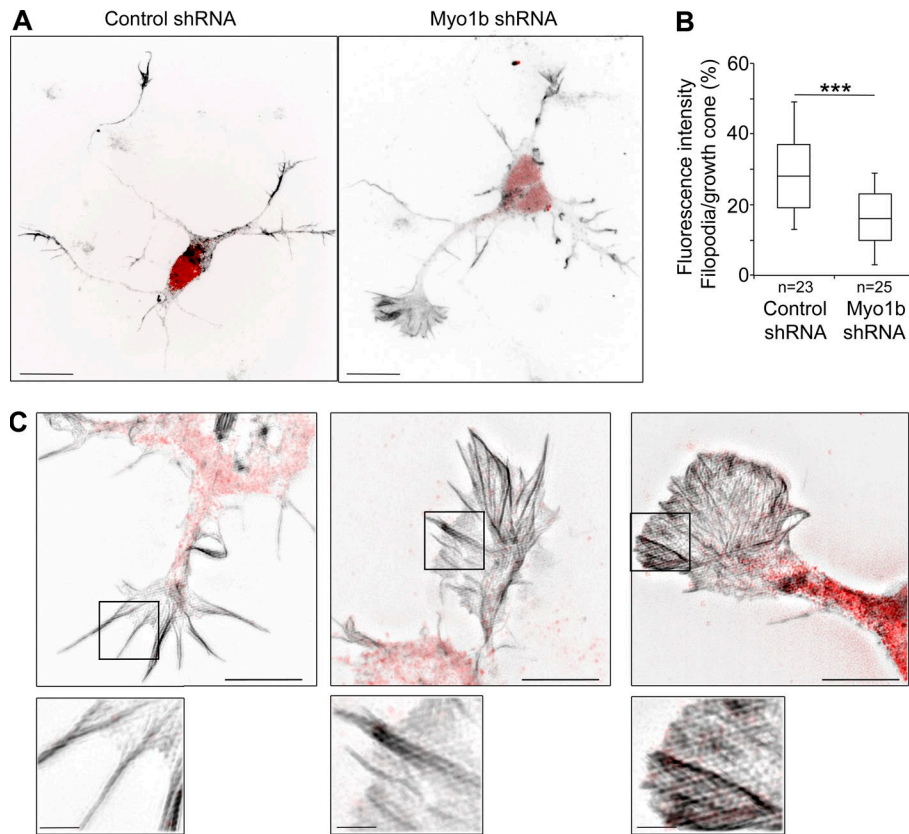


Figure 10. Myo1b depletion decreases F-actin in filopodia and increases F-actin in the interfilopodial veils. (A) Representative confocal z stacks of cortical neurons expressing control mCherry-shRNA or Myo1b-Cherry-shRNA and mGFP-F-tractin-P. Bars, 11 μ m. **(B)** The fluorescent intensity of F-actin within the area occupied by filopodia has been quantified on all sections of the stacks and normalized to the fluorescent intensity measured on the area occupied by the total growth cone on all sections and represented as box plots. $n = 23$ or 25 in three independent experiments. Data distribution was assumed to be normal. Unpaired t test. **, $P < 0.01$. **(C)** Cortical neurons transfected with plasmid encoding control mCherry-shRNA or Myo1b-mCherry-shRNA (**B**) were analyzed with SIM. Representative merged images of growth cones showing F-actin (gray) and mCherry (red) are shown. Bars, 5 μ m.

this task. Indeed, knockout of myosin 1a in mouse produced herniation of the apical membrane of the enterocytes (Tyska et al., 2005; Diz-Muñoz et al., 2010), and we have recently reported that filopodia induced by EphB2/ephrin B1 signaling requires Myo1b (Prospéri et al., 2015). Thus, by linking mechanically actin bundles to the membrane, Myo1b may stabilize the filopodia in both actin waves and growth cones.

In conclusion, our data demonstrate that Myo1b controls the dynamics of actin waves and growth cones by mechanically coupling F-actin to the plasma membrane. Consequently Myo1b regulates actin wave migration, F-actin, and filopodia stability in both structures. As a result of its role in F-actin organization, Myo1b modulates indirectly microtubule distribution and microtubule-dependent transport, which are required to specify the future axon (Winans et al., 2016).

Materials and methods

Antibodies and reagents

The following antibodies were used: homemade anti-Myo1b polyclonal antibodies (Almeida et al., 2011), 1:1,000 for Western blot and 1:50 for immunofluorescence; mouse monoclonal antibodies against Tau-1 (1:100) purchased from EMD Millipore and β -3 tubulin (1:150) purchased from Abcam; and rabbit polyclonal anti-GAPDH (1:20,000 for Western blot) purchased from Sigma-Aldrich. We also used Alexa Fluor 488-, 546-, or 647-coupled secondary antibodies against mouse or rabbit IgG (1:400) and horseradish peroxidase-conjugated secondary antibodies against mouse or rabbit IgG (1:5,000; Invitrogen); and anti-rabbit

IgG Cy3 (1:400; Jackson ImmunoResearch Laboratories, Inc.; or 1:500; Molecular Probes). Alexa Fluor 488- or 546-conjugated phalloidin was used to detect F-actin (1:400; Invitrogen).

Neuronal culture and transfection

Dissociated cultures of cortical neurons were prepared as classically described for hippocampal neurons (Dotti et al., 1988). In brief, we removed the brains from E16 mouse embryos after sacrificing pregnant mice with cervical dislocation, and we dissected the cortices in HBSS (Thermo Fisher Scientific) supplemented with 0.5% glucose (timed pregnant OF1 mice from Charles River Laboratories). Cortices were dissociated in HBSS containing 0.5% glucose and 0.25% trypsin-EDTA (Thermo Fisher Scientific) for 18 min at 37°C. HBSS buffer was then replaced by DMEM supplemented by GlutaMAX (Gibco) and 10% fetal bovine serum, and the cortices were mechanically dissociated by gently pipetting in this buffer. Immediately after dissociation, neurons were collected and plated at 0.5×10^5 cell/cm² onto poly D-lysine-coated coverslips (0.100 mg/ml; 30,000–70,000 molecular weight; Sigma-Aldrich). After attachment of the neurons to the substrate (~8–10 h), the medium was changed to neurobasal medium (Gibco) containing 1% B27 supplement (Gibco), 0.25% GlutaMAX (Invitrogen), and 0.5% penicillin-streptomycin (Thermo Fisher Scientific). For longer cultures, the neurons were fed twice a week with freshly made culture media.

Cells were transfected by electroporation using the Amaxa mouse neuron nucleofactor kit (CN VPG-1001; Lonza) according to the manufacturer's instructions. In brief, $4.2\text{--}4.5 \times 10^6$ neurons were resuspended in 100 μ l of nucleofactor solution containing

2–2.5 μg of plasmid or 30 pmol of siRNA. After electroporation, they were plated at 0.9×10^5 cells on 18-mm coverslips or 0.75×10^5 on 12-mm coverslips for immunofluorescence labeling, 0.5×10^6 cells on glass-bottom 35-mm Fluorodish wells (World Precision Instruments) for live-imaging, or 4.2×10^6 cells in 35-mm plastic wells for Western blot.

cdNA constructs

Plasmids encoding EGFP-Myo1b, Flag-HA-Myo1b, and Flag-HA-Myo1b-5M with five silent mutations introduced in the siRNA target sequence 5'-GCCTATCTAGAGATTAACAAG-3' as well as Flag-HA-Myo1b-5MR generated by site-directed mutagenesis of the plasmid encoding Flag-HA-Myo1b-5M with the introduction of a N160A mutation have been reported previously (Almeida et al., 2011; Prospéri et al., 2015). EGFP-Myo1b-K966A was prepared by subcloning Myo1b K966A where Lys966, a conserved basic residue in the β 1-loop-2 motif, was replaced with alanine (Komaba and Coluccio, 2010) into pEGFP-C1 and p-mCherry-C1 plasmids. mCherry-Myo1b was prepared by subcloning EGFP-Myo1b into mCherry plasmid at EcoRI-SalI; pBa.Kif5c 1–559-EGFP was a gift from G. Banker (Oregon Health and Science University, Portland, OR; 45059; Addgene). Plasmids encoding LifeAct-mCherry and LifeAct-EGFP were gifts from G. Montagnac (Institut Curie, Paris, France; Riedl et al., 2008) and M. Piel (Institut Curie, Paris, France), respectively. pcDNA3-AKT-PH-EGFP was a gift from C. Montell (University of California, Santa Barbara, Santa Barbara, CA; 18836; Addgene). The plasmid encoding mGFP-F-tractin-P was a gift from J. Hammer III (National Institutes of Health, Bethesda, MD; Yi et al., 2012).

siRNAs and shRNAs

An in-house-designed Myo1b siRNA (5'-GCTTACCTGGAAATCAACAAG-3') and a nontargeting sequence designed by GE Healthcare used as control siRNA have been previously described (Almeida et al., 2011; Prospéri et al., 2015). The Myo1b shRNA sequence has been cloned by the company Capoeira in the Psi-mU6 vector, which expresses the reporter gene mCherryFP. The nontargeting sequence clone CSHCTRO01 was used as a control.

Immunofluorescence labeling for confocal and superresolution SIM microscopies

For confocal microscopy and SIM (Fig. 1), neurons were fixed in 4% PFA in PBS (pH 7.4) for 15 min at RT and permeabilized with 0.1% Triton X-100 for 5 min before antibody incubation using standard procedures. Neurons were incubated in primary antibodies in PBS for 1 h and washed three times with PBS. They were then incubated with secondary antibodies for 1 h in PBS and washed 3 times. F-actin was labeled with fluorescent phalloidin. Coverslips were mounted on Superfrost slides with Fluoromount-G mounting medium (SouthernBiotech).

For spinning confocal microscopy and SIM (Fig. 10), neurons were fixed using a protocol for the preservation of cytoskeletal structures (Bell and Safiejko-Mroczka, 1995). In brief, the cells were incubated for 10 min at RT in 1 mM dithiobis(succinimidyl) propionate in HBSS followed by 10 min at RT in 1 mM dithiobis(succinimidyl) propionate in microtubule stabilizing

buffer (MTSB) containing 1 mM EGTA, 4% polyethylene glycol (PEG 8000), and 100 mM Pipes, pH 6.9. Cells were then washed for 5 min in TSB (0.5% Triton X-100 in MTSB fixed by adding an equal volume of 4% PFA in MTSB at RT for 15 min. After a 5-min wash in PBS, cells were incubated in PBS + 100 mM glycine for 5 min and again washed for 5 min in PBS. Fixed cells were incubated in PBS containing 0.1% Triton X-100 for 5 min at RT before using standard procedures for immunofluorescence labeling as described above.

Immunoblotting

Proteins separated by SDS-PAGE were transferred to nitrocellulose membranes and processed for immunoblotting using Lumi-Light Western blotting substrate (Roche). Images of immunoblots were captured with CL-XPosure film (Thermo Fisher Scientific) within the linear range and quantified by densitometry using the Analyze gel function of ImageJ.

Drug treatments

1 μM PCIP (gift from H.-J. Knölker, Technische Universität Dresden, Dresden, Germany) in 0.1% DMSO (Sigma-Aldrich) was incubated for 15 min at 37°C before performing live-cell imaging for 1 h, or was incubated for 1 h at 37°C before fixation. Control experiments were monitored with 0.1% DMSO.

Platinum replica EM

Platinum replicas of the cytoskeleton of cortical neurons were prepared as previously described by Svitkina and Borisov (2006) with some modifications. Primary cultures of DIV2 were extracted for ~1 min in PEM buffer containing 0.25% Triton-X-100, 0.25% glutaraldehyde, 5 μM phalloidin, and 10 μM taxol, and fixed with 2% glutaraldehyde.

Specimens were postfixed with 0.1% tannic acid followed by 0.1% uranylacetate, dehydrated with graded series of ethanol, incubated in 0.1% uranylacetate in ethanol, and dried by critical point drying (EM CPD300; Leica). Dried specimens were sputter-coated with 2-nm platinum followed by carbon coating (EM ACE600; Leica). Replicas were mounted on EM grids and observed with a transmission electron microscope (Tecnaï Spirit; FEI) at 100 kV.

Light microscopy and image acquisition

Image acquisition and image analysis were performed on the workstation of the PICT-IBISA Lhomond imaging facility of Institut Curie. Immunofluorescence confocal microscopy (Figs. 1 C, 2 C, 3 A, and 8, A and C) was performed with an inverted laser-scanning confocal microscope (A1r; Nikon) equipped with a 60 \times 1.4 NA oil immersion objective. The means of z stacks using FIJI (ImageJ) are shown. For superresolution microscopy (Figs. 1 D, 4 [A and C], 5 A, and 10 C), acquisitions were performed in 3D SIM mode with an N-SIM Nikon microscope before image reconstruction using the NIS Elements viewer software (Nikon; Gustafsson, 2008). The system is equipped with a Plan Apochromat TIRF SR 100 \times 1.49 NA oil immersion objective, a laser illumination (488 nm, 200 mW; 561 nm, 100 mW; and 640 nm, 100 mW) camera, and an electron-multiplying charge-coupled device DU-897 camera (Andor Technology). Images were acquired as a z

stack (0.12 μm per step). Images were then reconstructed using Elements software. Spinning-disk confocal microscopy (Fig. 5, B and C; Fig. 6, A and B; Fig. 7, A–D; Fig. 9, A, B, F, and G; Fig. 10 A; Fig. S3, A–D; and Videos 1, 2, 3, 4, 5, 7, 8, 9, and 10) was performed with a spinning-disk head (CSU-X1; Yokogawa Electric Corp.) on a microscope (TI Nikon) equipped with a piezo stage (Mad City Labs), mounted on an XYZ-encoding motorized scanning stage with 60 \times or 100 \times 1.4 NA oil immersion objectives and an intensifier EM-charge-coupled device camera under 5% CO_2 and at 37°C. Time-lapse phase-contrast microscopy (Fig. S2 and Video 6) was performed with an Eclipse inverted microscope (Nikon) equipped with a 60 \times 1.3 NA oil immersion objective and a CoolSNAP HQ2 camera under 5% CO_2 and at 37°C. For long-term experiments, images were acquired every minute for 1 h. For short-term experiments, images were acquired every second for 3 min. Fluorescence image acquisition parameters varied depending on the particular experiment and were determined to balance signal intensity and minimize cellular toxicity. These microscopes were steered with MetaMorph (7.1; Universal Imaging Corp.).

Image analysis quantification and statistics

Morphometric analysis of neuronal shape parameters including neurite number, growth cone area, and the length of the longest neurite was performed by using the FIJI software plugin NeuronJ. Axons were defined as the longest process containing intermediate to high levels of Tau-1 as judged by immunofluorescence labeling (Schwamborn and Püschel, 2004). Neurons were counted with multiple axons when they displayed two or more long neurites that were immunostained for Tau-1. Actin waves were defined in fixed samples as F-actin-rich growth cone-like structures with filopodial and/or lamellipodial features along the neurite shaft. The frequencies of anterograde, retrograde, or abortive waves were visually identified and quantified on time-lapse images acquired for neurons at stage 2, or stage 2–3 transition at DIV1 by spinning-disk confocal microscopy. Kymographs were performed using the kymograph plugin in FIJI. The box and whisker plots are represented using Excel (Microsoft), and the number of data points used for the graphical representation is indicated on the figures. Statistical comparisons for Figs. 2 (D and G), 3 B, and 6 [C–H] were performed with the χ^2 test. Statistical comparisons for box plots were performed with the Mann-Whitney test using Exact Dynamic Programming Solution of the Wilcoxon-Mann-Whitney (EDISON-WMW) test. The single asterisks (*), double asterisks (**), and triple asterisks (***) in the bar graphs indicate p-values of <0.05, <0.01, and <0.001, respectively, and p-values >0.05 are indicated by NS.

Online supplemental material

Fig. S1, related to Figs. 5, 9, and 10, shows the efficiency of Myo1b depletion using siRNA. Fig. S2, related to Fig. 8, shows the impact of Myo1b depletion on the growth cone area. Fig. S3, related to Fig. 9, shows the impact of Myo1b depletion on filopodia in actin waves. Video 1, related to Fig. 5 B, shows the correlation between the propagation of an actin wave and the migration of Myo1b. Video 2, related to Fig. 5 C, shows the correlation between the migration of PIP3 and Myo1b along the neurite. Video 3, related to Fig. 6 (A and B), shows the impact of Myo1b depletion on actin

waves. Video 4, related to Fig. 7 (A and B), shows the impact of Myo1b depletion on Kif5C dynamics. Video 5, related to Fig. 7 (C and D), shows the impact of Myo1b overexpression on Kif5C dynamics. Video 6, related to Fig. S2, shows the impact of Myo1b depletion on the growth cones area. Video 7, related to Fig. 9 (A and B), shows the impact of Myo1b depletion using siRNA on filopodia of a growth cone. Video 8, related to Fig. 9 (F and G), shows the impact of Myo1b depletion using shRNA on filopodia of a growth cone. Video 9, related to Fig. S3 (A and B), shows the impact of Myo1b depletion using siRNA on filopodia of actin waves. Video 10, related to Fig. S3 (C and D), shows the impact of Myo1b depletion using shRNA on filopodia of actin waves.

Acknowledgments

We thank L. Sengmanivong, V. Fraissier, and L. Leconte from The Biomaging Cell and Tissue Core Facility of the Institut Curie and Nikon Imaging Center, Institut Curie, member of the French National Research Infrastructure France-BioImaging (ANR10-INBS-04).

This work has been supported by Institut Curie, Centre National de la Recherche Scientifique, and Agence Nationale de la Recherche (grant ANR-14-CE11-0005-03). E. Coudrier's group belongs to the Centre National de la Recherche Scientifique consortium CellTiss and to the Labex CelTisPhyBio (11-LBX-0038).

The authors declare no competing financial interests.

Author contributions: O. Iuliano designed, performed, and analyzed the majority of the experiments. A. Yoshimura and M.-T. Prospéri designed, performed, and analyzed some of the experiments. R. Martin and H.-J. Knölker synthesized PCIP. E. Coudrier supervised the project, wrote the manuscript, and provided the financial support.

Submitted: 28 March 2017

Revised: 20 December 2017

Accepted: 2 March 2018

References

- Almeida, C.G., A. Yamada, D. Tenza, D. Louvard, G. Raposo, and E. Coudrier. 2011. Myosin 1b promotes the formation of post-Golgi carriers by regulating actin assembly and membrane remodelling at the trans-Golgi network. *Nat. Cell Biol.* 13:779–789. <https://doi.org/10.1038/ncb2262>
- Bähler, M., R. Kroschewski, H.E. Stöfler, and T. Behrmann. 1994. Rat myr 4 defines a novel subclass of myosin I: Identification, distribution, localization, and mapping of calmodulin-binding sites with differential calcium sensitivity. *J. Cell Biol.* 126:375–389. <https://doi.org/10.1083/jcb.126.2.375>
- Bartlett, W.P., and G.A. Banker. 1984a. An electron microscopic study of the development of axons and dendrites by hippocampal neurons in culture. I. Cells which develop without intercellular contacts. *J. Neurosci.* 4:1944–1953.
- Bartlett, W.P., and G.A. Banker. 1984b. An electron microscopic study of the development of axons and dendrites by hippocampal neurons in culture. II. Synaptic relationships. *J. Neurosci.* 4:1954–1965.
- Bell, P.B. Jr., and B. Safiejko-Mroccka. 1995. Improved methods for preserving macromolecular structures and visualizing them by fluorescence and scanning electron microscopy. *Scanning Microsc.* 9:843–857, discussion: 858–860.
- Benesh, A.E., J.T. Fleming, C. Chiang, B.D. Carter, and M.J. Tyska. 2012. Expression and localization of myosin-1d in the developing nervous system. *Brain Res.* 1440:9–22. <https://doi.org/10.1016/j.brainres.2011.12.054>

- Bradke, F., and C.G. Dotti. 1999. The role of local actin instability in axon formation. *Science*. 283:1931–1934. <https://doi.org/10.1126/science.283.5409.1931>
- Brzeska, H., K. Pridham, G. Chery, M.A. Titus, and E.D. Korn. 2014. The association of myosin IB with actin waves in dictyostelium requires both the plasma membrane-binding site and actin-binding region in the myosin tail. *PLoS One*. 9:e94306. <https://doi.org/10.1371/journal.pone.0094306>
- Chapman, B.V., A.I. Wald, P. Akhtar, A.C. Munko, J. Xu, S.P. Gibson, J.R. Grandis, R.L. Ferris, and S.A. Khan. 2015. MicroRNA-363 targets myosin IB to reduce cellular migration in head and neck cancer. *BMC Cancer*. 15:861. <https://doi.org/10.1186/s12885-015-1888-3>
- Chinthalapudi, K., M.H. Taft, R. Martin, S.M. Heissler, M. Preller, F.K. Hartmann, H. Brandstaetter, J. Kendrick-Jones, G. Tsiavalariis, H.O. Gutzeit, et al. 2011. Mechanism and specificity of pentachloropseudilin-mediated inhibition of myosin motor activity. *J. Biol. Chem.* 286:29700–29708. <https://doi.org/10.1074/jbc.M111.239210>
- Diz-Muñoz, A., M. Krieg, M. Bergert, I. Ibarlucea-Benitez, D.J. Muller, E. Paluch, and C.P. Heisenberg. 2010. Control of directed cell migration in vivo by membrane-to-cortex attachment. *PLoS Biol.* 8:e1000544. <https://doi.org/10.1371/journal.pbio.1000544>
- Dotti, C.G., C.A. Sullivan, and G.A. Banker. 1988. The establishment of polarity by hippocampal neurons in culture. *J. Neurosci.* 8:1454–1468.
- Flynn, K.C., C.W. Pak, A.E. Shaw, F. Bradke, and J.R. Bamberg. 2009. Growth cone-like waves transport actin and promote axonogenesis and neurite branching. *Dev. Neurobiol.* 69:761–779. <https://doi.org/10.1002/dneu.20734>
- Gustafsson, M.G. 2008. Super-resolution light microscopy goes live. *Nat. Methods*. 5:385–387. <https://doi.org/10.1038/nmeth0508-385>
- Inagaki, N., M. Toriyama, and Y. Sakumura. 2011. Systems biology of symmetry breaking during neuronal polarity formation. *Dev. Neurobiol.* 71:584–593. <https://doi.org/10.1002/dneu.20837>
- Jacobson, C., B. Schnapp, and G.A. Banker. 2006. A change in the selective translocation of the Kinesin-1 motor domain marks the initial specification of the axon. *Neuron*. 49:797–804. <https://doi.org/10.1016/j.neuron.2006.02.005>
- Kakumoto, T., and T. Nakata. 2013. Optogenetic control of PIP3: PIP3 is sufficient to induce the actin-based active part of growth cones and is regulated via endocytosis. *PLoS One*. 8:e70861. <https://doi.org/10.1371/journal.pone.0070861>
- Kawano, Y., T. Yoshimura, D. Tsuboi, S. Kawabata, T. Kaneko-Kawano, H. Shirataki, T. Takenawa, and K. Kaibuchi. 2005. CRMP-2 is involved in kinesin-1-dependent transport of the Sra-1/WAVE1 complex and axon formation. *Mol. Cell Biol.* 25:9920–9935. <https://doi.org/10.1128/MCB.25.22.9920-9935.2005>
- Komaba, S., and L.M. Coluccio. 2010. Localization of myosin Ib to actin protrusions requires phosphoinositide binding. *J. Biol. Chem.* 285:27686–27693. <https://doi.org/10.1074/jbc.M109.087270>
- Korobova, F., and T. Svitkina. 2008. Arp2/3 complex is important for filopodia formation, growth cone motility, and neuriteogenesis in neuronal cells. *Mol. Biol. Cell*. 19:1561–1574. <https://doi.org/10.1091/mbc.E07-09-0964>
- Laakso, J.M., J.H. Lewis, H. Shuman, and E.M. Ostap. 2008. Myosin I can act as a molecular force sensor. *Science*. 321:133–136. <https://doi.org/10.1126/science.1159419>
- Lewis, A.K., and P.C. Bridgman. 1996. Mammalian myosin I alpha is concentrated near the plasma membrane in nerve growth cones. *Cell Motil. Cytoskeleton*. 33:130–150. [https://doi.org/10.1002/\(SICI\)1097-0169\(1996\)33:2%3C130::AID-CM5%3E3.0.CO;2-G](https://doi.org/10.1002/(SICI)1097-0169(1996)33:2%3C130::AID-CM5%3E3.0.CO;2-G)
- Lewis, T.L. Jr., J. Courchet, and F. Polleux. 2013. Cell biology in neuroscience: Cellular and molecular mechanisms underlying axon formation, growth, and branching. *J. Cell Biol.* 202:837–848. <https://doi.org/10.1083/jcb.201305098>
- McIntosh, B.B., and E.M. Ostap. 2016. Myosin-I molecular motors at a glance. *J. Cell Sci.* 129:2689–2695. <https://doi.org/10.1242/jcs.186403>
- Nambiar, R., R.E. McConnell, and M.J. Tyska. 2009. Control of cell membrane tension by myosin-I. *Proc. Natl. Acad. Sci. USA*. 106:11972–11977. <https://doi.org/10.1073/pnas.0901641106>
- Nambiar, R., R.E. McConnell, and M.J. Tyska. 2010. Myosin motor function: the ins and outs of actin-based membrane protrusions. *Cell Mol. Life Sci.* 67:1239–1254. <https://doi.org/10.1007/s00018-009-0254-5>
- Neukirchen, D., and F. Bradke. 2011. Neuronal polarization and the cytoskeleton. *Semin. Cell Dev. Biol.* 22:825–833. <https://doi.org/10.1016/j.semdcb.2011.08.007>
- Nishimura, T., K. Kato, T. Yamaguchi, Y. Fukata, S. Ohno, and K. Kaibuchi. 2004. Role of the PAR-3-KIF3 complex in the establishment of neuronal polarity. *Nat. Cell Biol.* 6:328–334. <https://doi.org/10.1038/ncb1118>
- Ohmura, G., T. Tsujikawa, T. Yaguchi, N. Kawamura, S. Mikami, J. Sugiyama, K. Nakamura, A. Kobayashi, T. Iwata, H. Nakano, et al. 2015. Aberrant Myosin Ib Expression Promotes Cell Migration and Lymph Node Metastasis of HNSCC. *Mol. Cancer Res.* 13:721–731. <https://doi.org/10.1158/1541-7786.MCR-14-0410>
- Prospéri, M.T., P. Lépine, F. Dingli, P. Paul-Gilloteaux, R. Martin, D. Loew, H.J. Knölker, and E. Coudrier. 2015. Myosin Ib functions as an effector of EphB signaling to control cell repulsion. *J. Cell Biol.* 210:347–361. <https://doi.org/10.1083/jcb.201501018>
- Randlett, O., L. Poggi, F.R. Zolessi, and W.A. Harris. 2011. The oriented emergence of axons from retinal ganglion cells is directed by laminin contact in vivo. *Neuron*. 70:266–280. <https://doi.org/10.1016/j.neuron.2011.03.013>
- Raposo, G., M.N. Cordonnier, D. Tenza, B. Menichi, A. Dürrbach, D. Louvard, and E. Coudrier. 1999. Association of myosin I alpha with endosomes and lysosomes in mammalian cells. *Mol. Biol. Cell*. 10:1477–1494. <https://doi.org/10.1091/mbc.10.5.1477>
- Ren, Y., and D.M. Suter. 2016. Increase in Growth Cone Size Correlates with Decrease in Neurite Growth Rate. *Neural Plast.* 2016:3497901. <https://doi.org/10.1155/2016/3497901>
- Riedl, J., A.H. Crevenna, K. Kessenbrock, J.H. Yu, D. Neukirchen, M. Bista, F. Bradke, D. Jenne, T.A. Holak, Z. Werb, et al. 2008. Lifeact: a versatile marker to visualize F-actin. *Nat. Methods*. 5:605–607. <https://doi.org/10.1038/nmeth.1220>
- Ruppert, C., J. Godel, R.T. Muller, R. Kroschewski, J. Reinhard, and M. Bahler. 1995. Localization of the rat myosin I molecules myr 1 and myr 2 and in vivo targeting of their tail domains. *J. Cell Sci.* 108:3775–3786.
- Ruthel, G., and G. Banker. 1998. Actin-dependent anterograde movement of growth-cone-like structures along growing hippocampal axons: a novel form of axonal transport? *Cell Motil. Cytoskeleton*. 40:160–173. [https://doi.org/10.1002/\(SICI\)1097-0169\(1998\)40:2%3C160::AID-CM5%3E3.0.CO;2-J](https://doi.org/10.1002/(SICI)1097-0169(1998)40:2%3C160::AID-CM5%3E3.0.CO;2-J)
- Ruthel, G., and G. Banker. 1999. Role of moving growth cone-like “wave” structures in the outgrowth of cultured hippocampal axons and dendrites. *J. Neurobiol.* 39:97–106. [https://doi.org/10.1002/\(SICI\)1097-4695\(199904\)39:1%3C97::AID-NEU8%3E3.0.CO;2-Z](https://doi.org/10.1002/(SICI)1097-4695(199904)39:1%3C97::AID-NEU8%3E3.0.CO;2-Z)
- Salas-Cortes, L., F. Ye, D. Tenza, C. Wilhelm, A. Theos, D. Louvard, G. Raposo, and E. Coudrier. 2005. Myosin Ib modulates the morphology and the protein transport within multi-vesicular sorting endosomes. *J. Cell Sci.* 118:4823–4832. <https://doi.org/10.1242/jcs.02607>
- Sapir, T., T. Levy, A. Sakakibara, A. Rabinkov, T. Miyata, and O. Reiner. 2013. Shootin1 acts in concert with KIF20B to promote polarization of migrating neurons. *J. Neurosci.* 33:11932–11948. <https://doi.org/10.1523/JNEUROSCI.5425-12.2013>
- Schwamborn, J.C., and A.W. Püschel. 2004. The sequential activity of the GTPases Rap1B and Cdc42 determines neuronal polarity. *Nat. Neurosci.* 7:923–929. <https://doi.org/10.1038/nn1295>
- Sherr, E.H., M.P. Joyce, and L.A. Greene. 1993. Mammalian myosin I α , I β , and I γ : New widely expressed genes of the myosin I family. *J. Cell Biol.* 120:1405–1416. <https://doi.org/10.1083/jcb.120.6.1405>
- Svitkina, T.M., and G.G. Borisov. 2006. Correlative light and electron microscopy of the cytoskeleton; d. J. Celis, In *Cell Biology: A Laboratory Handbook*. Third edition. Vol. 3. Academic Press, San Diego. 277–285.
- Toriyama, M., T. Shimada, K.B. Kim, M. Mitsuba, E. Nomura, K. Katsuta, Y. Sakumura, P. Roepstorff, and N. Inagaki. 2006. Shootin1: A protein involved in the organization of an asymmetric signal for neuronal polarization. *J. Cell Biol.* 175:147–157. <https://doi.org/10.1083/jcb.200604160>
- Tyska, M.J., A.T. Mackey, J.D. Huang, N.G. Copeland, N.A. Jenkins, and M.S. Mooseker. 2005. Myosin-Ia is critical for normal brush border structure and composition. *Mol. Biol. Cell*. 16:2443–2457. <https://doi.org/10.1091/mbc.E04-12-1116>
- Winans, A.M., S.R. Collins, and T. Meyer. 2016. Waves of actin and microtubule polymerization drive microtubule-based transport and neurite growth before single axon formation. *eLife*. 5:e12387. <https://doi.org/10.7554/eLife.12387>
- Yamada, A., A. Mamane, J. Lee-Tin-Wah, A. Di Cicco, C. Prévost, D. Lévy, J.F. Joanny, E. Coudrier, and P. Bassereau. 2014. Catch-bond behaviour facilitates membrane tubulation by non-processive myosin Ib. *Nat. Commun.* 5:3624. <https://doi.org/10.1038/ncomms4624>
- Yi, J., X.S. Wu, T. Crites, and J.A. Hammer III. 2012. Actin retrograde flow and actomyosin II arc contraction drive receptor cluster dynamics at the immunological synapse in Jurkat T cells. *Mol. Biol. Cell*. 23:834–852. <https://doi.org/10.1091/mbc.E11-08-0731>